R. & M. No. 3646

R. & M. No. 3646

MINISTRY OF TECHNOLOGY
AERONAUTICAL RESEARCH COUNCIL
REPORTS AND MEMORANDA

Calculation of the Turbulent Boundary Layer in a Vortex Diffuser

By T-S CHAM and M. R. HEAD

Cambridge University Engineering Department

LONDON: HER MAJESTY'S STATIONERY OFFICE
1970
PRICE 16*s.* 0*d.* [80p] NET

Calculation of the Turbulent Boundary Layer in a Vortex Diffuser

By T-S CHAM and M. R. HEAD

Cambridge University Engineering Department

Reports and Memoranda No. 3646*
May, 1969

Summary.

In two-dimensional potential flow the combination of a source and a free vortex produces an axis-symmetric flow with streamlines in the form of equiangular spirals. Calculations have been made of the turbulent boundary layer developing beneath such a flow and the results have been compared with measurements made elsewhere.

The method of calculation used is essentially that described earlier by Cumpsty and Head, integral equations of momentum and entrainment being satisfied in a streamline co-ordinate system.

LIST OF CONTENTS

*Replaces A.R.C. 31 237.

1. *Introduction.*

In two-dimensional potential flow, the combination of a source and a vortex produces streamlines which take the form of equiangular spirals, the angle being determined by the ratio of the strengths of the source and the vortex. Such a flow is approximated in practice by that occurring in a so-called vaneless diffuser. The boundary layer that develops on the diffuser wall is fully three-dimensional, being affected both by divergence and by the crossflow which results from the curvature of the external streamlines. The development of the boundary layer has a great effect on the efficiency of the diffuser, and if the pressure rise is large separation may occur. The present calculations therefore deal with a case of some practical significance.

This problem was selected for study because the mainstream imposes an adverse pressure gradient on the boundary layer and large crossflows are generated. Moreover, experiments by Gardow[1] provide several sets of measurements with which the results of the calculations can be compared.

Gardow investigated the three-dimensional turbulent boundary layer on the wall of a vaneless diffuser with different values of the swirl angle at inlet. This was controlled by varying the rate of rotation of a cylindrical wire screen at inlet, as indicated in Fig. 1. Jansen[2] continued Gardow's work but with the interest extended to the whole regime of flow between the diffuser walls. His theoretical analysis of the problem assumed fixed power laws for the mean velocity profiles and was so closely adapted to this particular problem that it is difficult to see how it could be applied to a general three-dimensional turbulent boundary layer.

The method used in the present calculation is similar to that of Cumpsty and Head[3]. It makes use of

two momentum integral equations, one in the streamwise and one in the crossflow direction, and an equation of entrainment.

2. *Co-ordinate System.*

2.1. *Preliminary.*

In three-dimensional boundary-layer problems, it is important to choose the co-ordinate system best suited to the case under consideration. Sometimes considerable simplification of the analysis can be achieved by considering the geometry of the body or that of the external flow.

In general, the most convenient co-ordinate system is that related to the external streamlines. Such a choice leads to simple boundary conditions and has other advantages, as pointed out by Cumpsty and Head[3]. However, it does mean that an initial calculation of the external streamlines and their orthogonal trajectories is necessary. In principle, this can be carried out by 'measuring' distances along streamlines, curvatures and divergence of streamlines, etc., but considerable time and effort can be saved if reasonably simple analytical expressions can be found for the external streamlines and their orthogonal family. The required information can then be easily extracted.

2.2. *Co-ordinate System based on Logarithmic Spirals and their Orthogonal Family.*

The combination of a free vortex flow, $v_\theta = C_2/r$, and a source flow, $v_r = C_1/r$, is a logarithmic spiral flow where v_r and v_θ are the radial velocity and tangential velocity respectively, r is the radius and C_1, C_2 are constants. The resultant velocity vector makes a constant angle α with the circumferential direction, where $\tan\alpha = C_1/C_2$, as shown in Figure 1.

The differential equation of a streamline is

$$\frac{1}{r}\frac{dr}{d\theta} = \tan\alpha = \text{constant } (a, \text{say}).$$

On integration, $r = C\exp(a\theta)$, where C is the integration constant.

By choosing different values for the constant C, a family of logarithmic spirals is generated. It can then be deduced that the family of orthogonal trajectories to these spirals is

$$r = D\exp(-\theta/a),$$

where D is the family parameter. It may be noted that the constant a depends on the swirl angle for the particular case considered.

To define the co-ordinate system fully, a radial reference line must be chosen for $\theta = 0$. Referring to Figure 2, the streamline η can then be identified as the spiral which meets this reference line at a radial distance η. Similarly, the potential line ξ can be defined as the trajectory orthogonal to the spirals which meets $\theta = 0$ at $r = \xi$. By defining ζ as the actual distance measured perpendicular to the plane of (ξ, η), a right-hand orthogonal curvilinear co-ordinate system is formed. It may be noted that by such a definition of the co-ordinate system, ξ and η have dimensions of length.

2.3. *Properties of the Streamline Co-ordinate System.*

For any general orthogonal curvilinear co-ordinate system ξ, η on the surface of a body, the distance between adjacent lines of constant ξ or η will vary from point to point. The actual distance measured along the surface relating to incrementals in ξ and η is given by

$$ds^2 = h_1^2\,d\xi^2 + h_2^2\,d\eta^2$$

where s is the actual distance on the surface, and h_1 and h_2 are the Lamé coefficients (which in this case are dimensionless).

It is necessary to determine h_1 and h_2 as functions of ξ and η. To evaluate h_1, integration is carried out on the streamline η to obtain the distance along the path between (ξ, η) and $(\xi + d\xi, \eta)$.

The equation of the streamline is $r = \eta \exp(a\theta)$, and since

$$s = \pm\sqrt{r^2 + (dr/d\theta)^2}\, d\theta,$$

$$\text{the elemental length } h_1 d\xi = \int_{\theta_1}^{\theta_2} \sqrt{\eta^2 e^{2a\theta} + a^2 \eta^2 e^{2a\theta}}\, d\theta$$

where θ_1 and θ_2 are the angles corresponding to points (ξ, η) and $(\xi + d\xi, \eta)$.

The details of the integration are given in the Appendix.

$$\text{It is shown that } h_1 = \frac{a}{\sqrt{1+a^2}} \left(\frac{\eta}{\xi}\right)^{1/(a^2+1)}.$$

To evaluate h_2, the integration is carried out along the potential line ξ

$$h_2 d\eta = \int_{\theta_1}^{\theta_3} \sqrt{r^2 + (dr/d\theta)^2}\, d\theta$$

where θ_3 now corresponds to the position $(\xi, \eta + d\eta)$. As shown in the Appendix

$$h_2 = \frac{1}{\sqrt{a^2+1}} \left(\frac{\xi}{\eta}\right)^{a^2/(a^2+1)}.$$

As h_1 and h_2 are explicitly functions of ξ and η, the convergence and curvatures are simply the appropriate partial differentials. It may also be noted that this method of evaluating h_1 and h_2 is different in details from that of Cumpsty and Head[3], and is more convenient for this particular case.

The expression for the external velocity U can also be simply obtained in terms of ξ and η.

$$\text{Since } U = \sqrt{(C_1^2 + C_2^2)}/r = C_2\sqrt{1+a^2}/r,$$

it can be shown that on a streamline,

$$U = C_2\sqrt{1+a^2}\,(\eta)^{-1/(a^2+1)}(\xi)^{-a^2/(a^2+1)}.$$

Two useful expressions are then

$$\frac{1}{U}\frac{\partial U}{\partial \xi} = -\frac{a^2}{a^2+1}(\xi)^{-1}$$

$$\text{and} \quad \frac{1}{U}\frac{\partial U}{\partial \eta} = -\frac{1}{a^2+1}(\eta)^{-1}.$$

2.4. *Simplification of Analysis due to Radial Symmetry.*

Consider a function $f(\xi, \eta)$ of the flow. By definition

$$\frac{\partial f}{\partial \eta} = \underset{\Delta\eta \to 0}{\text{Limit}} \left[\frac{f(\xi, \eta + \Delta\eta) - f(\xi, \eta)}{\Delta\eta}\right].$$

If the flow has radial symmetry, it is true that $f(\xi_0, \eta_0+d\eta) = f(\xi_0+d\xi, \eta_0)$ provided that the points $(\xi_0, \eta_0+d\eta)$ and $(\xi_0+d\xi, \eta_0)$ are at the same radial distance from the origin.

Referring to Fig. 2, it is easily seen that points B and D are equidistant from the origin provided angle BDA is equal to α, the swirl angle.

Therefore, the condition is

$$\frac{h_2\, d\eta}{h_1\, d\xi} = \tan\alpha, \quad \text{from which}$$

$$\frac{d\xi}{d\eta} = \frac{1}{a^2}\left(\frac{\xi}{\eta}\right).$$

Hence, with radial symmetry,

$$\frac{\partial f}{\partial \eta} = \underset{\Delta\eta \to 0}{\text{Limit}} \left[\frac{f(\xi+d\xi, \eta)-f(\xi, \eta)}{\Delta\xi} \cdot \frac{\Delta\xi}{\Delta\eta}\right].$$

But as $\Delta\eta \to 0$, $\Delta\xi \to 0$ if the ratio $\dfrac{\Delta\xi}{\Delta\eta} = \dfrac{1}{a^2}\left(\dfrac{\xi}{\eta}\right)$ is kept constant.

Hence
$$\frac{\partial f}{\partial \eta} = \frac{1}{a^2}\left(\frac{\xi}{\eta}\right)\frac{\partial f}{\partial \xi}. \tag{1}$$

Thus, all the crossflow derivatives can be transformed to streamwise derivatives by the use of the above equation. It may be noted that it is entirely a geometrical property, the exact form of which is determined by the manner in which the co-ordinate system is defined.

3. *Basic Equations.*

3.1. *Momentum Equations.*

By similar arguments to those employed in two dimensions, the turbulent boundary-layer equations are the same as the laminar equations with the addition of Reynolds shear stresses and the steady velocities replaced by time-means. If u, v, w are to represent the mean velocities in the directions ξ, η, ζ, respectively, the equations of motion are (*see* Cooke and Hall[4])

$$\frac{u}{h_1}\frac{\partial u}{\partial \xi}+\frac{v}{h_2}\frac{\partial u}{\partial \eta}+w\frac{\partial u}{\partial \xi}-K_2\, uv+K_1\, v^2 = -\frac{1}{\rho}\frac{1}{h_1}\frac{\partial p}{\partial \xi}+\frac{1}{\rho}\frac{\partial \tau_1}{\partial \zeta} \tag{2}$$

$$\frac{u}{h_1}\frac{\partial v}{\partial \xi}+\frac{v}{h_2}\frac{\partial v}{\partial \eta}+w\frac{\partial v}{\partial \xi}-K_1\, uv+K_2\, u^2 = -\frac{1}{\rho}\frac{1}{h_2}\frac{\partial p}{\partial \eta}+\frac{1}{\rho}\frac{\partial \tau_2}{\partial \zeta} \tag{3}$$

where K_1 and K_2 are the geodesic curvatures.

$$K_1 = -\frac{1}{h_1 h_2}\frac{\partial h_2}{\partial \xi}, \qquad K_2 = -\frac{1}{h_1 h_2}\frac{\partial h_1}{\partial \eta}.$$

The equation in the ζ direction is of little interest as, by the boundary layer approximation, it merely states that the pressure difference across the boundary-layer is negligible.

The continuity equation is

$$\frac{\partial}{\partial \xi}(h_2\, u)+\frac{\partial}{\partial \eta}(h_1\, v)+\frac{\partial}{\partial \zeta}(h_1\, h_2\, w) = 0. \tag{4}$$

By integrating (2) and (3) from 0 to h, where $h \geqslant \delta$, and using equation (4), the momentum integral equations for a three-dimensional boundary layer are obtained.

The integral equations are (*see* Cooke and Hall[4])

$$\frac{1}{h_1 U^2}\frac{\partial}{\partial \xi}(\theta_{11} U^2)+\frac{1}{h_2 U^2}\frac{\partial}{\partial \eta}(\theta_{12} U^2)+\frac{1}{h_1 U}\frac{\partial U}{\partial \xi}\delta_1^*-\frac{1}{h_2 U}\frac{\partial U}{\partial \eta}\delta_2^*$$

$$-K_1(\theta_{11}+\theta_{22})-K_2(\theta_{12}-\theta_{21})=\frac{\tau_{o1}}{\rho U^2} \tag{5}$$

$$-\frac{1}{h_1 U^2}\frac{\partial}{\partial \xi}(\theta_{21} U^2)-\frac{1}{h_2 U^2}\frac{\partial}{\partial \eta}(\theta_{22} U^2)-K_1(\theta_{12}-\theta_{21}-\delta_2^*)$$

$$+K_2(\theta_{22}+\theta_{11}+\delta_1^*)=\frac{\tau_{o2}}{\rho U^2} \tag{6}$$

where

$$\delta_1^*=\frac{1}{U}\int_0^\delta (U-u)d\xi \qquad \delta_2^*=\frac{1}{U}\int_0^\delta v\,d\zeta$$

$$\theta_{11}=\frac{1}{U^2}\int_0^\delta (U-u)u\,d\zeta \qquad \theta_{21}=\frac{1}{U^2}\int_0^\delta vu\,d\zeta$$

$$\theta_{12}=\frac{1}{U^2}\int_0^\delta (U-u)v\,d\zeta \qquad \theta_{22}=\frac{1}{U^2}\int_0^\delta v^2\,d\zeta$$

and τ_{o1} and τ_{o2} are the wall shear stresses in the streamwise and crossflow direction respectively.

On substituting the relevant expressions obtained previously and putting $b^2 = a^2+1$, the momentum integral equations can be simplified to

$$ab^2\frac{\partial \theta_{11}}{\partial \xi}+b^2\xi\frac{\partial \theta_{12}}{\partial \xi}+a^3(\theta_{22}-\theta_{11}-\delta_1^*)+a^2(\delta_2^*-\theta_{12}-\theta_{21})=(\eta)^{1/b^2}(\xi)^{a^2/b^2}a^2 b\frac{\tau_{o1}}{\rho U^2} \tag{7}$$

and

$$-ab^2\xi\frac{\partial \theta_{21}}{\partial \xi}-b^2\xi\frac{\partial \theta_{22}}{\partial \xi}+a^3(\theta_{21}+\theta_{12}-\delta_2^*)+a^2(\theta_{22}-\theta_{11}-\delta_1^*)=(\eta)^{1/b^2}(\xi)^{a^2/b^2}a^2 b\frac{\tau_{o2}}{\rho U^2}. \tag{8}$$

It may be noted that equations (7) and (8) contain derivatives in the streamwise direction only. (*See* transformation equation (1)).

3.2. *Entrainment Equation.*

The momentum integral equations are not of course sufficient to determine the development of the turbulent boundary layer and an auxiliary equation is required. The one used here is an extension of Head's entrainment equation for the two-dimensional case to one of three dimensions.

Consider the control volume making up the boundary layer between streamlines η and $\eta+d\eta$ and between potential lines ξ and $\xi+d\xi$, as shown in Fig. 2. Let Q_1 be the volume flow per unit width of the boundary layer in the streamwise direction at (ξ, η) and Q_2 be the quantity in the crossflow direction.

Applying continuity consideration to the control volume, the volume of fluid entrained, dQ, is given by

$$dQ = h_2\, d\eta\left[\frac{\partial Q_1}{\partial \xi}\, d\xi + Q_1 \frac{1}{h_2}\frac{\partial h_2}{\partial \xi}\, d\xi\right] + h_1\, d\xi\left[\frac{\partial Q_2}{\partial \eta}\, d\eta + Q_2 \frac{1}{h_1}\frac{\partial h_1}{\partial \eta}\, d\eta\right].$$

It may be noted that, of the four terms on the right-hand side, the first is due to the change in flow rate Q_1 with ξ, the second is due to streamline divergence, the third represents the change in flow rate Q_2 with η, and the fourth is due to streamline curvature.

For a three-dimensional boundary layer,

$$Q_1 = U(\delta - \delta_1^*) \qquad \text{and} \qquad Q_2 = \int_0^\delta v\, d\zeta = U\delta_2^*.$$

If C_E is the non-dimensional entrainment coefficient,

$$C_E = \frac{dQ}{U h_1 h_2\, d\xi\, d\eta}$$

$$\equiv \frac{1}{U}\left[\frac{1}{h_1}\frac{\partial\, U(\delta-\delta_1^*)}{\partial \xi} + \frac{U(\delta-\delta_1^*)}{h_1 h_2}\frac{\partial h_2}{\partial \xi} + \frac{1}{h_2}\frac{\partial (U\delta_2^*)}{\partial \eta} + \frac{\delta_2^*}{h_1 h_2}\frac{\partial h_1'}{\partial \eta}\right].$$

On substituting the relevant terms into the above expression, the entrainment equation becomes

$$ab^2\,\xi\frac{\partial(\delta-\delta_1^*)}{\partial \xi} + b^2\,\xi\frac{\partial \delta_2^*}{\partial \xi} - a^2\,\delta_2^* + a\,\delta_2^* = (\eta)^{1/b^2}\,(\xi)^{a^2/b^2}\; a^2 b\, C_E. \tag{9}$$

C_E is to be determined by the streamwise velocity component of the turbulent boundary layer. Therefore in its three-dimensional equivalent,

$$C_E = C_E\left[\frac{\delta - \delta_1^*}{\theta_{11}}\right].$$

4. *Assumptions.*

4.1. *Streamwise Profiles.*

It is assumed that the streamwise velocity profiles correspond to Thompson's[6] two-dimensional profile family where $\frac{u}{U} = \frac{u}{U}(H, R_\theta, y/\theta)$ the two-dimensional momentum thickness θ being replaced by the streamwise momentum thickness θ_{11}. It has been shown by Thompson that his two-parameter family provides a good representation of two-dimensional turbulent boundary-layer profiles over a wide range of conditions.

4.2. *Crossflow Profiles.*

It is assumed that the crossflow corresponds to the form suggested by Mager[7]

$$\frac{v}{u} = \tan\beta\,(1-\zeta/\delta)^2,$$

where β is the angle between the surface streamline and the projection of the external streamline upon the surface. The crossflow model also suggests that

$$\tan\beta = \operatorname*{Lim}_{\zeta \to 0}\left(\frac{v}{u}\right) = \frac{\tau_{o2}}{\tau_{o1}}.$$

Although it has been stated (e.g. Johnston[8]) that this model does not give an accurate representation of turbulent boundary-layer crossflow, it remains a very convenient form for use with the momentum integral equation, and does in fact give fair agreement with many cases of crossflow provided a proper choice is made of the limiting angle β at the wall.

4.3. *Skin Friction.*

The streamwise skin friction is calculated using Thompson's skin-friction relation $C_f = C_f(R_\theta, H)$, the two-dimensional momentum thickness θ being replaced by the streamwise momentum thickness θ_{11}. This relationship follows from his profile family.

4.4. *Crossflow Thicknesses.*

As the crossflow using Mager's form does not depend critically on the exact streamwise velocity distribution, a more convenient form than Thompson's has been used for calculating the crossflow thicknesses. An nth power streamwise velocity profile is chosen consistent with the shape factor H, and the crossflow thus calculated is almost identical with one using Thompson's velocity profile. This was also shown by Cumpsty and Head[3].

4.5. *Entrainment Relations.*

It is assumed that the magnitude of the crossflow has negligible effect on the rate of entrainment and that it is entirely determined by the velocity defect of the streamwise component of the mean velocity. By this assumption, it can be argued from dimensional considerations as by Head[5] that entrainment is a function of $H_{\delta-\delta_1^*}$. However, it is found that in order to obtain results having good agreement with the experiments, a new curve of entrainment with $H_{\delta-\delta_1^*}$ has to be assumed, as shown in Fig. 4. The relationship between H and $H_{\delta-\delta^*}$ given by Head[5] has been used in the present calculation.

5. *Cases Treated.*

As the object of the theoretical analysis was to compare the calculated developments of the three-dimensional turbulent layers with the experimental results, the constants used in the present theory had been chosen such that the theoretical models were kept as close as possible to the actual experiments performed by Gardow[1] at M.I.T.

The dimensions of Gardow's experimental set-up of the diffuser walls are shown in Fig. 1. The rotating screens had an open area ratio of approximately 50 per cent and were driven at rotational speeds of 800 rpm to 1410 rpm. There was a series of 11 ports on the diffuser wall for the measurement of velocity profiles by means of a three-hole cobra-probe.

Three sets of experimental data were used and they were renamed as Sets 1, 2 and 3 which correspond to Gardow's Runs A 45·2, B 50·6 and B 54·5. They were chosen for comparison because the measurements made were the most comprehensive. They represented different initial swirl angles and inlet velocities, as shown in the table below.

Set	Inlet Swirl Angle (α)	Inlet Velocity (ft/sec)	Screen Speed (RPM)	Volume Flow (CFM)
1	44·8	40·1	900	2135
2	39·4	43·9	900	2070
3	35·5	53·2	1000	1980

Because of the limited distance between the two walls of the diffuser and the effect of boundary-layer growth, the external flow did not conform closely to the ideal source-vortex flow.

An attempt was made to adjust the theory to fit the experimental streamlines but this proved to be too complicated in the subsequent analysis. Finally, it was decided to adopt the theoretical logarithmic spiral path for the flow at the edge of the boundary layer but to use this in conjunction with the measured radial pressure gradient. It was also necessary to assume the angle of swirl to be the mean of the angles measured at the first and last stations. As shown by the comparisons between calculated and experimental results (Section 7), this treatment was found to be satisfactory.

6. *Details of Calculation.*

The main equations for the calculation are the streamwise momentum integral equation (7), the crossflow momentum integral equation (8), and the entrainment equation (9).

The initial conditions (i.e. H, $R_{\theta 11}$ and β) were deduced from the experiments. The starting values of θ_{11} and δ_2^* were taken directly from the report, at a time when there was some uncertainty regarding the initial H in view of the experimental scatter. Fortunately, the calculation method is insensitive to the initial assumption of H, as the solutions are similar after a few step lengths downstream as shown in Fig. 12. The calculation of the development of the boundary layer was based on an overall iteration procedure. The streamwise development was first calculated using the streamwise momentum integral equation (7) and the entrainment equation with crossflow neglected. This first approximation to the streamwise development was then used to obtain a first approximation to the crossflow using equation (8). The crossflow was then included in equation (7) to improve the solution for the streamwise development. Successively improved approximations were then obtained by using the equations alternately. It was seldom necessary to go beyond five iterations before two successive iterations gave practically identical results.

The advantage of this method of solution is the stability of the iteration procedure, as was also indicated by Cumpsty and Head[3]. Again, by the very nature of the method of interpolating at the centre of the step length, the computer solution is smooth as shown in a typical computer output chart in Figs. 5 to 7, which are for Set 3. The step length throughout the $\Delta\xi = 0{\cdot}2$ which is also shown in the figures for ζ between 40 and 44. Provided the interpolation procedure is carried out properly, the step length is not critical in this method of solution.

7. *Comparisons with Experiment and Discussion.*

Values of the shape factor H for the streamwise velocity profile, as reported by Gardow[1], showed enormous scatter when plotted against radius. As a smooth variation would be expected, the experimental H values were recalculated from the measured velocity profiles. Care was taken to ensure that, near the wall, the velocity distribution was compatible with the skin friction as deduced from the combination of H and $R_{\theta 11}$ using Thompson's skin friction chart. The recalculated H values showed a much more tolerable scatter as will be seen from Figs. 10, 12 and 14.

The development of the mementum thickness in the streamwise direction for the three sets of observations is shown in Figs. 8a and 8b. The agreement between theory and experiment can be considered perfect by the standards normally accepted for turbulent boundary layers. The momentum thickness Reynolds number $R_{\theta 11}$ corresponding to Set 1 at the initial station was only 375. This is rather low for a normal turbulent layer but, possibly because of turbulence generated by the rotating screen, there is no doubt that the boundary layer was fully turbulent.

Fig. 9 shows the development of the crossflow thickness δ_2^*. For Sets 1 and 2, the agreement is very good, and while the theory is slightly on the low side in Set 3, it can still be considered satisfactory.

The surface yaw angle β is a quantity that is difficult to measure accurately, partly because the velocities near the surface are very small but also, and more important, because the finite size of the pressure tubes prevents yaw measurements being taken sufficiently close to the wall for actual surface values to be deduced. Moreover, there is no reason to suppose that the velocity vectors in the sublayer are collateral, as would be implied by Johnston's model[8] of the crossflow. This problem has been examined by Cham[9] and the conclusion is reached that substantial variations in crossflow may in fact take place through the sublayer. In view of the uncertainties, the theoretical calculations of the surface flow direction may be

considered to be in satisfactory agreement with the experimental values as reported by Gardow, as shown in Figs. 11, 13 and 15.

Some comparisons between calculated and experimental velocity profiles are shown in Figs. 17 to 21. It will be seen that the theoretical streamwise velocity profiles, as represented by Thompson's two-dimensional profile family, fit the experimental results very well, in spite of the large yaw angles. The theoretical crossflow velocity profiles based on a Mager model also give good overall agreement with the measurements. These results substantially justify the assumptions made for representing streamwise and crossflow velocity profiles, and support the principle of working in terms of these component velocities.

An attempt was made to compare the calculated skin-friction component in the streamwise direction with experimental values. Unfortunately, no direct measurements of the wall shear stress had been made, and the values reported by Gardow were deduced from a Clauser[10] plot with modification by Johnston[8]. The comparison for Sets 2 and 3 are shown in Fig. 16. Considering the uncertainties not only in the experimental skin-friction values but also in the surface yaw angles, the agreement must be considered satisfactory.

With the assumed $C_E, H_{\delta-\delta^*}$ curve the calculations appear to give a good account, in fact of every aspect of the development of the turbulent boundary layer in the diffuser.

8. *Conclusions.*

An analytical method has been found convenient for calculating the streamline co-ordinate system for the three-dimensional boundary-layer problem of flow in a free-vortex diffuser. The use of an entrainment equation together with the streamwise and the crossflow momentum integral equations enabled the development of the turbulent boundary layer to be simply calculated.

Based on the assumption that the entrainment rate depends only on the streamwise component of the velocity profile, increased rates of entrainment compared with those given by Head's curve for two dimensions were required to give the best agreement between theory and experiment. When this adjustment was made, the developments of the shape factor H, the streamwise momentum thickness θ_{11} and the crossflow thickness δ_2^* all showed good agreements with the experimental values.

The streamwise and crossflow velocity profiles were found to be well represented by Thompson's two parameter profile family and Mager's crossflow model respectively.

Although the external streamlines in the experiments were not perfect logarithmic spirals, it was still possible to carry out the calculation using this as an approximation, but with measured pressure gradients replacing the theoretical values. Where the difference between the experimental inlet and outlet swirl angles was large, a mean swirl angle was assumed for the calculation.

The good overall agreement between the calculations and experiment justifies many of the assumptions that are essential to the theory, but the problem of making a suitable *a priori* choice of entrainment curve remains to be solved.

9. *Additional Note.*

Since the foregoing was written an improved version of the original entrainment method has been developed[11]. This introduces a dependence of C_E on the parameter $\frac{1}{U}\frac{d(U\theta)}{dx}$, or more precisely, on the ratio $\frac{1}{U}\frac{d(U\theta)}{dx}\Big/\left[\frac{1}{U}\frac{d(U\theta)}{dx}\right]_{\text{eq}}$, where the denominator represents the value of $\frac{1}{U}\frac{d(U\theta)}{dx}$ for the equilibrium layer having the same values of H and R_θ. This dependence results in an increase of entrainment when the rate of growth of the layer is small and a decrease when it is large.

It will be recalled that the original curve relating C_E to $H_{\delta-\delta^*}$ was obtained empirically from two sets of measurements for layers proceeding to separation. Thus in two-dimensional flow the original method gives reasonably accurate predictions of H development in strong adverse pressure gradients, where H is increasing more or less rapidly, but fails to do so where H is either substantially constant (except in the flat-plate case) or decreasing. In these circumstances, values of C_E given by the original curve are appreciably too low. In the recent version of the method, the additional dependence of C_E on rate of growth has

eliminated this defect, and numerous comparisons with experiment show uniformly satisfactory agreement with measurements in separating layers, equilibrium layers and relaxing layers.

In the three-dimensional case treated in the present report we should in fact expect the original $C_E, H_{\delta-\delta^*}$ curve to underestimate the entrainment very considerably, first because we are dealing with an equilibrium flow and second, because divergence of the external streamlines leads to a further reduction in $\frac{1}{U}\frac{d(U\theta)}{dx}$. There is thus every reason to expect that, in this case, the more recent version of the method would give satisfactory agreement with experiment, without the necessity for arbitrary adjustments of the entrainment.

If we consider the results for other rotating flows (*see* Fig. 22) which have been treated in the same way as the present one (i.e. by the use of the original entrainment method with an adjusted C_E curve), we may reasonably conclude that the increased entrainment on the rotating cylinder at high values of the rotation parameter is adequately accounted for by centrifugal effects, and in Ref. 12 it is shown in fact that this increase can be reasonably well predicted. At low rates of rotation the flow is only trivially different from that on a flat plate (so long as the boundary layer is thin) and both the original and more recent versions of the entrainment method should give equally satisfactory results.

When we come to the rotating-disc case[13], however, where it is necessary to reduce the flat-plate C_E values by about one-third to secure complete agreement with experiment, we must consider the physical basis for the dependence of C_E upon $\frac{1}{U}\frac{d(U\theta)}{dx}$ that has been introduced in the more recent version of the entrainment method. This is discussed at some length in ref. 11, but here we may briefly point out that a high rate of growth, due to either a rapid retardation of the flow or strong flow convergence, will lead to a crowding-up of the large eddies of turbulence and consequently to a decrease in entrainment (as compared to the corresponding equilibrium case), while a low rate of growth, due to either a reduced pressure gradient or divergence of the flow will result in a separation of the large eddies, a more irregular outer boundary and an increase in entrainment.

Now, in the rotating-disc case, although there is no boundary-layer growth in the direction of the external streamlines, and no convergence, since the external streamlines are concentric circles, the large eddies will nonetheless be closely packed, because they will (presumably) be continuously formed in much the same way as in flat-plate flow, but instead of being swept downstream at something like stream velocity, will now be convected away radially at only a small fraction of the circumferential velocity. Thus we may expect on physical grounds that the entrainment should be reduced, as in fact it is, but the growth parameter $\frac{1}{U}\frac{d(U\theta)}{dx}$ now has no relevance, since in this particular problem it is in no way related to the closeness of packing of the large eddies. Thus there is no reason to expect that the more recent method should give an improved solution in this rather special case.

Acknowledgement.

The Additional Note was written at the suggestion of Mr. P. Bradshaw while the second author was Visiting Professor at I.I.T. Kanpur, India. Mr. Bradshaw's interest is gratefully acknowledged.

LIST OF SYMBOLS

v_θ	Tangential velocity
v_r	Radial velocity
C_1, C_2, a, b, C, D	Constants specifying the external flow
α	Swirl angle (*see* Fig. 1)
ξ, η, ζ	Curvilinear co-ordinates
s	Distance measured on the surface
h_1, h_2	Lamé coefficients
r, θ	Plane polar co-ordinates
f	Function
K_1, K_2	Geodesic curvatures
τ_1, τ_2	Components of shear stress in ξ and η directions
u, v, w	Mean velocity components within the boundary layer in the ξ, η, ζ directions
p	Pressure
ρ	Density
$\delta_1^*, \delta_2^*, \theta_{11}, \theta_{21}, \theta_{12}, \theta_{22}$	Three-dimensional boundary-layer thicknesses defined in Section 3.1
Q, Q_1, Q_2	Volume flow rates
U	Free-stream velocity
C_E	Entrainment coefficient
H	Shape parameter of streamwise velocity profile ($= \delta_1^*/\theta_{11}$)
$R_\theta, R_{\theta 11}$	Reynolds number based on streamwise momentum thickness
β	Angle between surface streamline and external streamline directions
τ_{o1}, τ_{o2}	Components of wall shear stress in ξ and η directions
C_f, C_{f1}	Coefficients of wall shear stress component in the streamwise direction
$H_{\delta - \delta_1}^*$	Form parameter ($= (\delta - \delta_1^*)/\theta_{11}$).

REFERENCES

No.	*Author(s)*	*Title, etc.*
1	E. B. Gardow	The three-dimensional turbulent boundary layer in a free vortex diffuser. M.I.T. Gas Turbine Lab. Report No. 42, 1958.
2	W. Jansen	Incompressible fluid flow in a radial vaneless diffuser. M.I.T. Gas Turbine Lab. Report No. 52, 1959.
3	N. A. Cumpsty and M. R. Head	The calculation of three-dimensional turbulent boundary layers, Pts. I and II. *Aero. Quart*, Vol. 18, p. 55 and p. 150, 1967.
4	J. C. Cooke and M. G. Hall ..	Boundary layers in three dimensions. *Progress in Aeronautical Sciences*, Vol. 2. Pergamon Press. 1962.
5	M. R. Head	Entrainment in the turbulent boundary layer. A.R.C. R. & M. 3152, 1958.
6	B. G. J. Thompson ..	A new two-parameter family of mean velocity profiles for incompressible turbulent boundary layers on smooth walls. A.R.C. R. & M. 3463, 1965.
7	A. Mager	Generalisation of boundary-layer mementum integral equations to three-dimensional flows including those of rotating systems. NACA Report 1067, 1952.
8	J. P. Johnston	On the three-dimensional turbulent boundary-layer generated by secondary flow. *ASME J. of Basic Engineering*, Vol. 82, p. 233, 1960.
9	T-S Cham	Turbulent boundary layers in rotating flows. Ph. D. Thesis, Cambridge University, 1968.
10	F. H. Clauser	Turbulent boundary layers in adverse pressure gradients. *J. Aero. Sci.* Vol. 21, p. 91, 1954.
11	M. R. Head and V. C. Patel ..	Improved entrainment method for calculating turbulent boundary-layer development. A.R.C. R. & M. 3643, 1969.
12	T-S Cham and M. R. Head ..	Turbulent boundary layer on a rotating cylinder in an axial stream. *J. Fluid Mech.* Vol. 42, p. 1, 1970.
13	T-S Cham and M. R. Head ..	Turbulent boundary-layer flow on a rotating disc. *J. Fluid Mech.* Vol. 37, p. 129, 1969.

APPENDIX

Details of Integrations to Obtain the Lamé Coefficients h_1 and h_2.

To evaluate h_1:

On streamline η, the elemental length $h_1\, d\xi$ is given by

$$h_1\, d\xi = \pm \int_{\theta_1}^{\theta_2} \sqrt{\eta^2\, e^{2a\theta} + a^2\, \eta^2\, e^{2a\theta}}\, d\theta\,,$$

where θ_1, θ_2 are the angles subtended by (ξ, η) and $(\xi + d\xi, \eta)$.

Since the radial distance at (ξ, η) can be given either by $\xi\, e^{-\theta/a}$ or by $\eta\, e^{\theta/a}$, it is easily deduced that

$$\theta_1 = \frac{1}{a + 1/a} \log \frac{\xi}{\eta}. \qquad \text{Similarly, } \theta_2 = \frac{1}{a + 1/a} \log \frac{\xi + d\xi}{\eta}.$$

Therefore,

$$h_1\, d\xi = \int_{\theta_1}^{\theta_2} \eta\, e^{a\theta} \sqrt{1 + a^2}\, d\theta$$

$$= \frac{\eta \sqrt{1 + a^2}}{a} \Big[\, e^{a\theta} \,\Big]_{\theta_1}^{\theta_2}$$

$$= \frac{\eta \sqrt{1 + a^2}}{a} \left[\exp\left\{ a \left(\frac{a}{a^2 + 1} \log \frac{\xi + d\xi}{\eta} \right) \right] \right.$$

$$\left. - \exp\left\{ a \left(\frac{a}{a^2 + 1} \log \frac{\xi}{\eta} \right) \right\} \right]$$

$$= \frac{\eta \sqrt{1 + a^2}}{a} \left[\left(\frac{\xi}{\eta} \right)^{\frac{a^2}{a^2 + 1}} \left\{ 1 + \frac{d\xi}{\xi} \right\}^{\frac{a^2}{a^2 + 1}} - \left(\frac{\xi}{\eta} \right)^{\frac{a^2}{a^2 + 1}} \right.$$

$$= \frac{\eta \sqrt{1 + a^2}}{a} \left(\frac{\xi}{\eta} \right)^{\frac{a^2}{a^2 + 1}} \frac{a^2}{a^2 + 1} \frac{d\xi}{\xi} + \cdots\cdots$$

$$\text{Hence } h_1 = \frac{a}{\sqrt{1 + a^2}} \left(\frac{\eta}{\xi} \right)^{\frac{1}{a^2 + 1}}.$$

To evaluate h_2:

For this purpose, the path of integration is along the potential line ξ.

$$h_2\, d\eta = \pm \int_{\theta_1}^{\theta_3} \sqrt{\xi^2\, e^{-\frac{2\theta}{a}} + \frac{\xi^2}{a^2} e^{-\frac{2\theta}{a}}}\, d\theta$$

where θ_3 is now for the point $(\xi, \eta + d\eta)$.

Hence,

$$h_2\, d\eta = \xi\sqrt{1+1/a^2}\int_{\theta_1}^{\theta_3} e^{-\frac{\theta}{a}}\, d\theta$$

$$= \xi\sqrt{1+a^2}\left[\ e^{-\frac{\theta}{a}}\ \right]_{\theta_1}^{\theta_3}$$

$$= \xi\sqrt{1+a^2}\left[\left(\frac{\xi}{\eta+d\eta}\right)^{-\frac{1}{a^2+1}} - \left(\frac{\xi}{\eta}\right)^{-\frac{1}{a^2+1}}\right]$$

$$= \xi\sqrt{1+a^2}\left[\left(\frac{\eta}{\xi}\right)^{\frac{1}{a^2+1}}\frac{1}{a^2+1}\,\frac{d\eta}{\eta} + \ldots.\right]$$

and

$$h_2 = \frac{1}{\sqrt{a^2+1}}\left(\frac{\xi}{\eta}\right)^{\frac{a^2}{a^2+1}}.$$

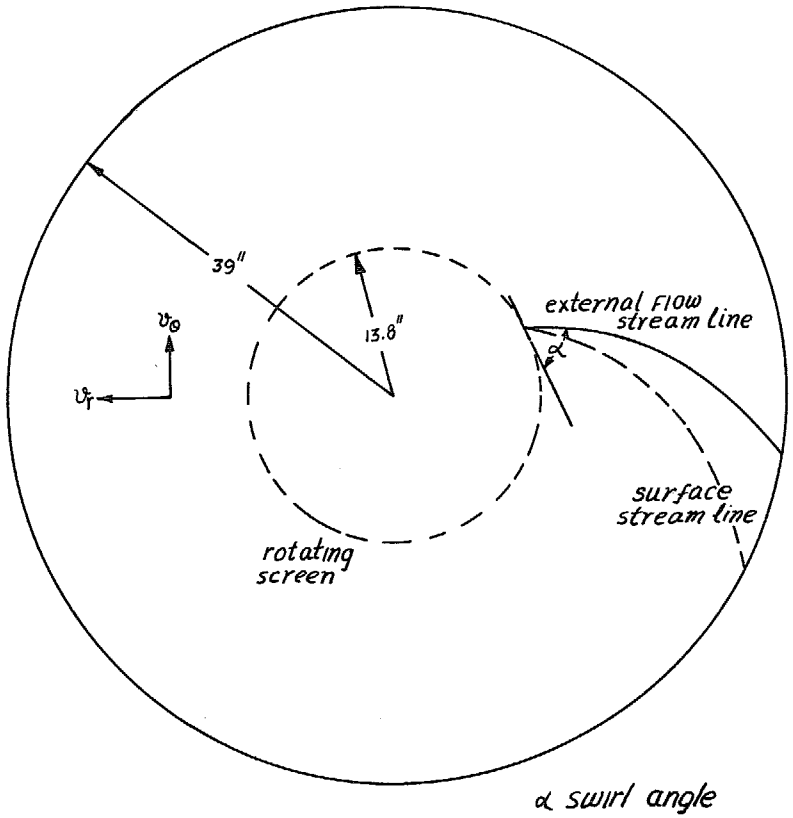

FIG. 1. Test section of free-vortex diffuser, Gardow[1].

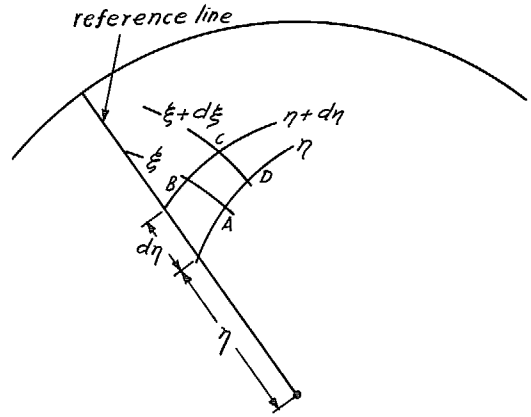

FIG. 2. Currilinear co-ordinate system.

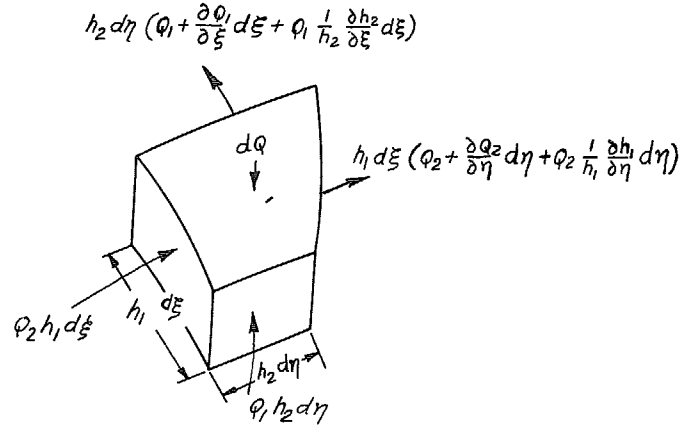

FIG. 3. Control volume for derivation of entrainment equation.

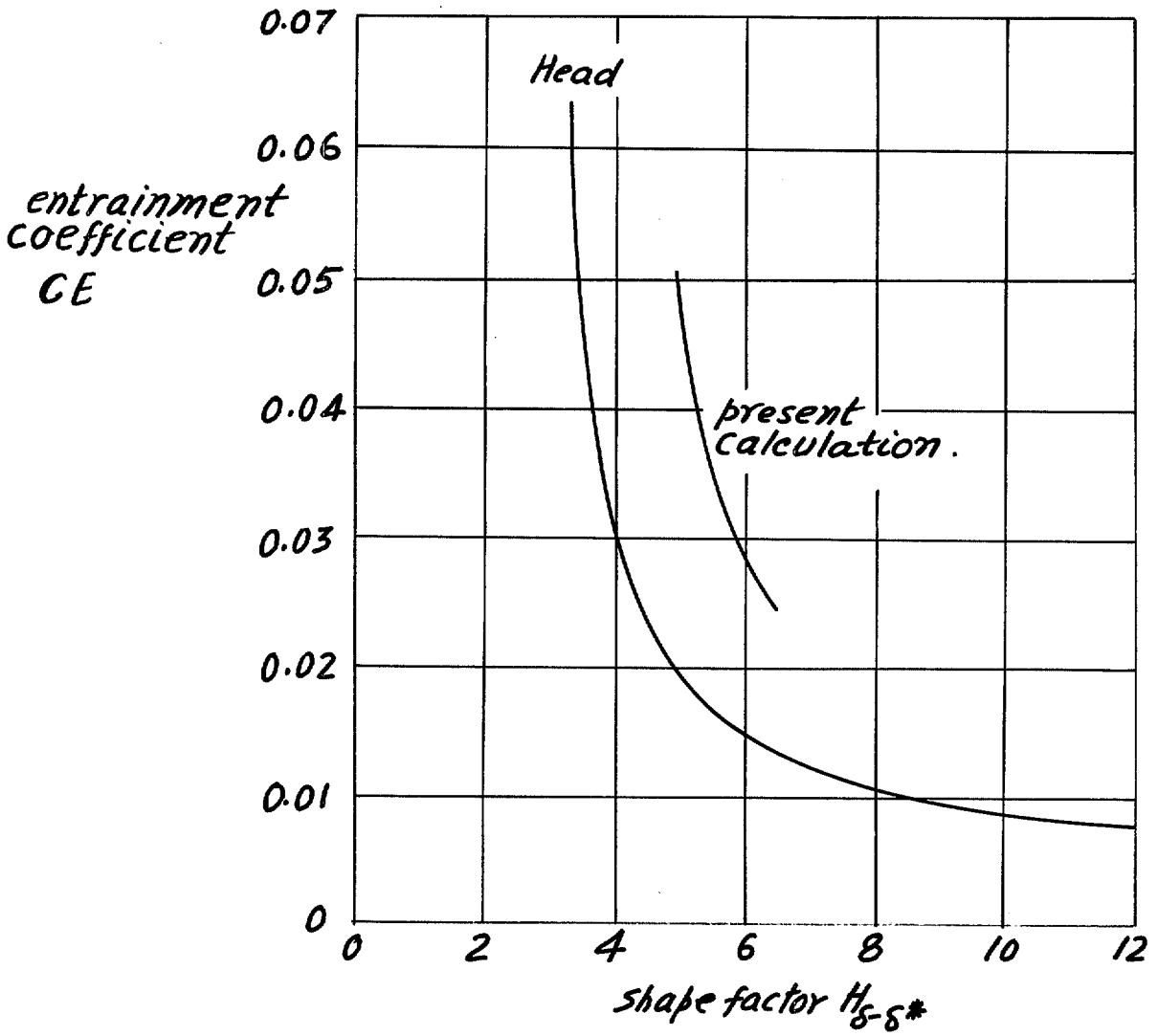

FIG. 4. Entrainment function used for calculation.

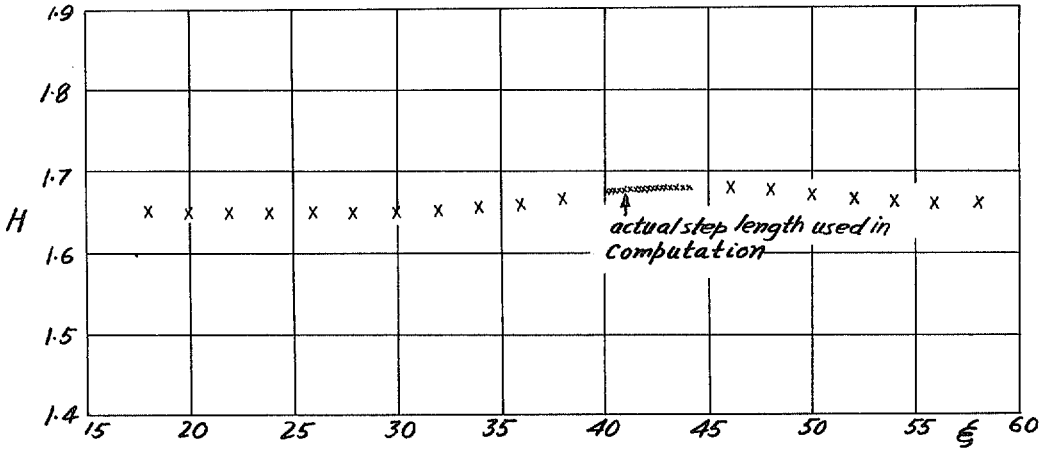

FIG. 5. Computer output for streamwise shape factor calculation, Set 3.

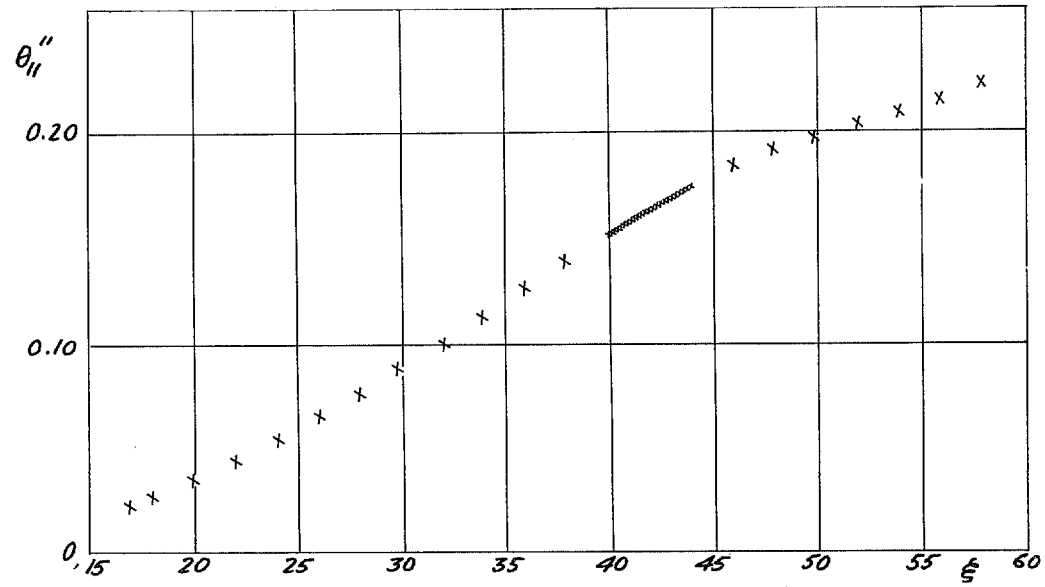

FIG. 7. Computer output for crossflow thickness calculation, Set 3.

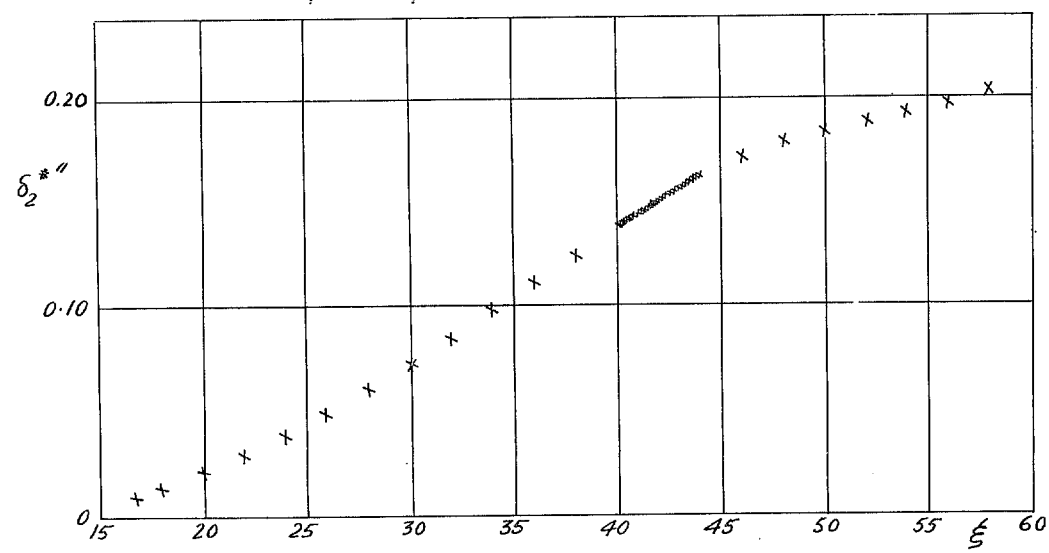

FIG. 6. Computer output for streamwise momentum thickness calculation, Set 3.

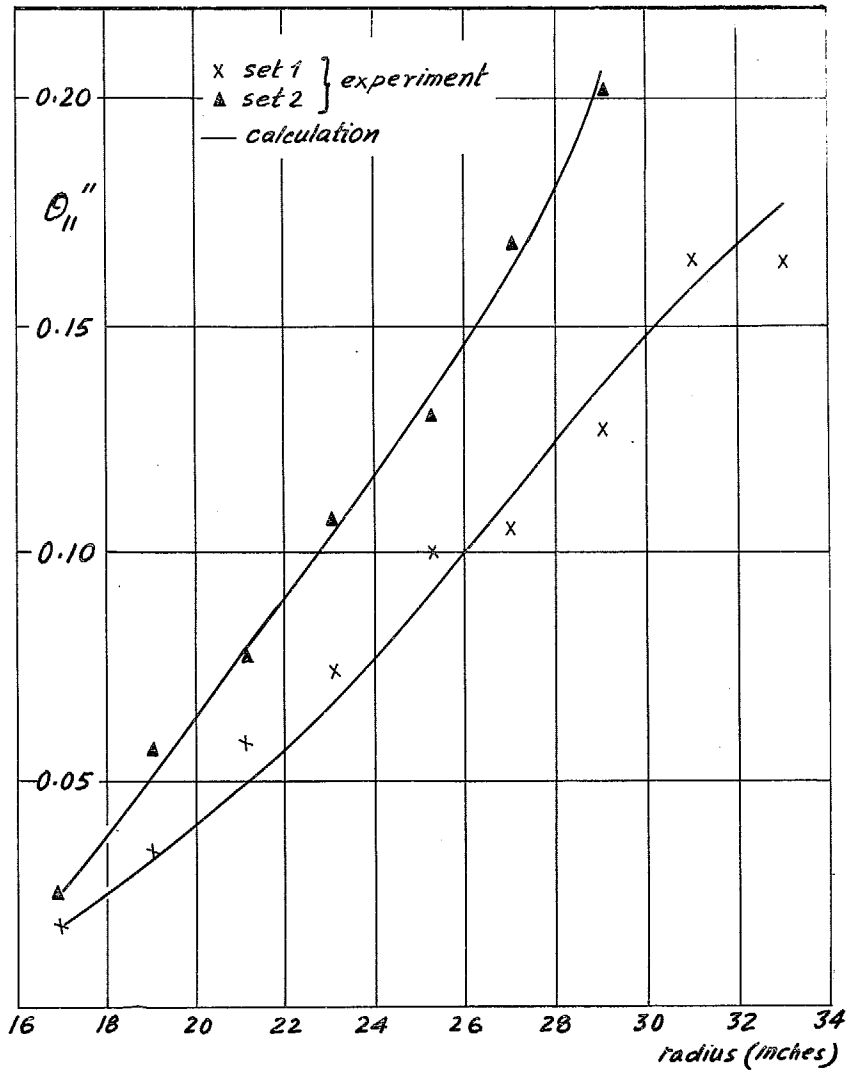

FIG. 8(a). Streamwise momentum thickness, Sets 1 and 2.

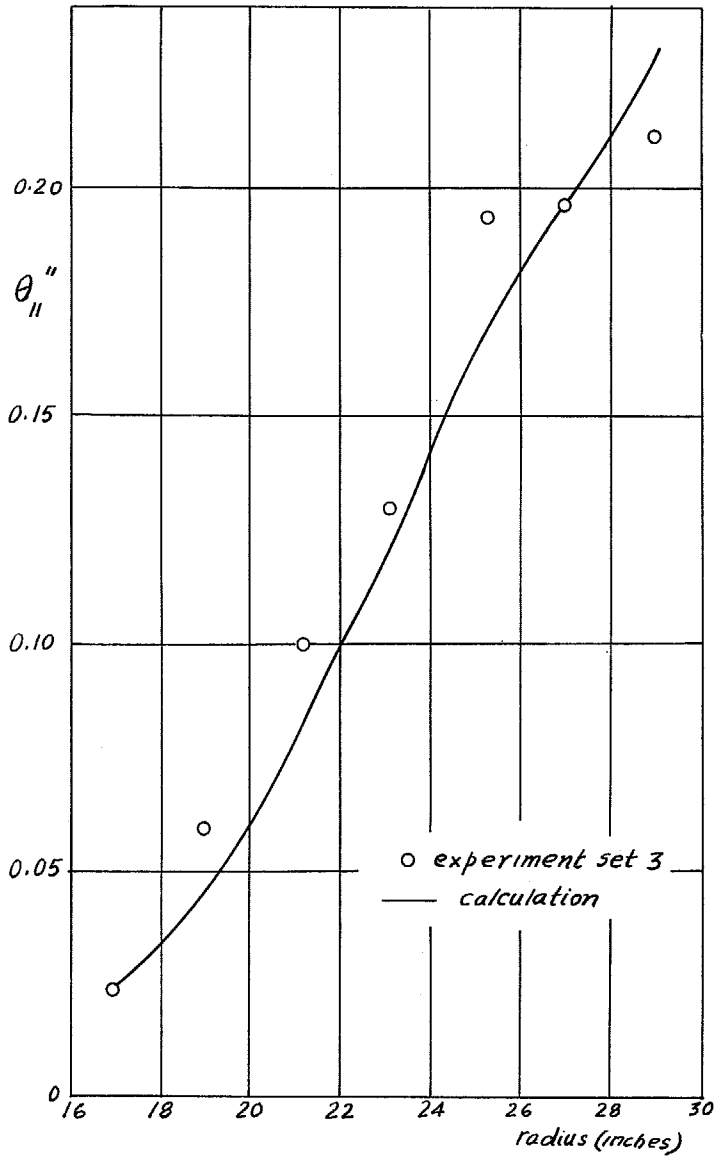

FIG. 8(b). Streamwise momentum thickness, Set 3.

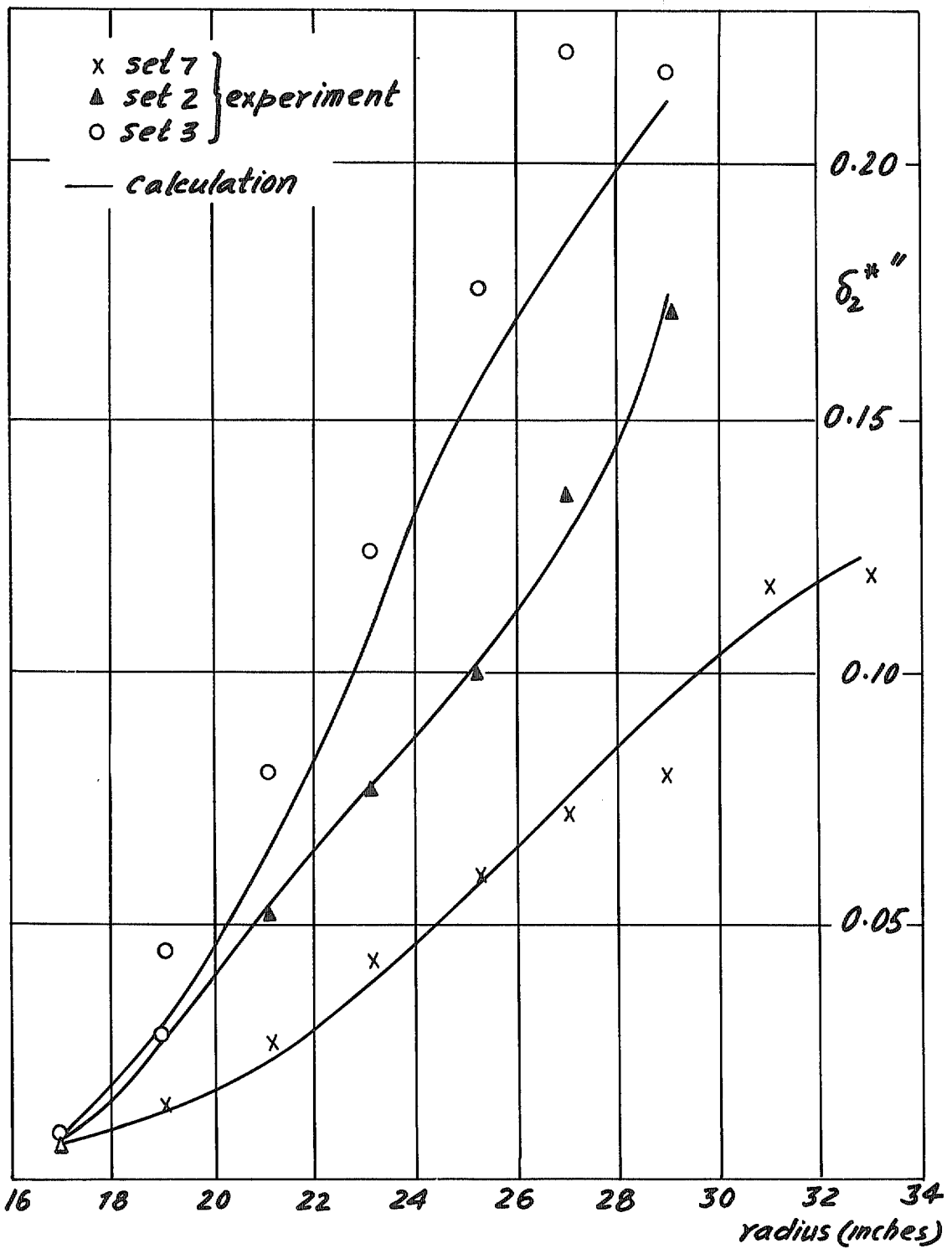

FIG. 9. Development of crossflow thickness.

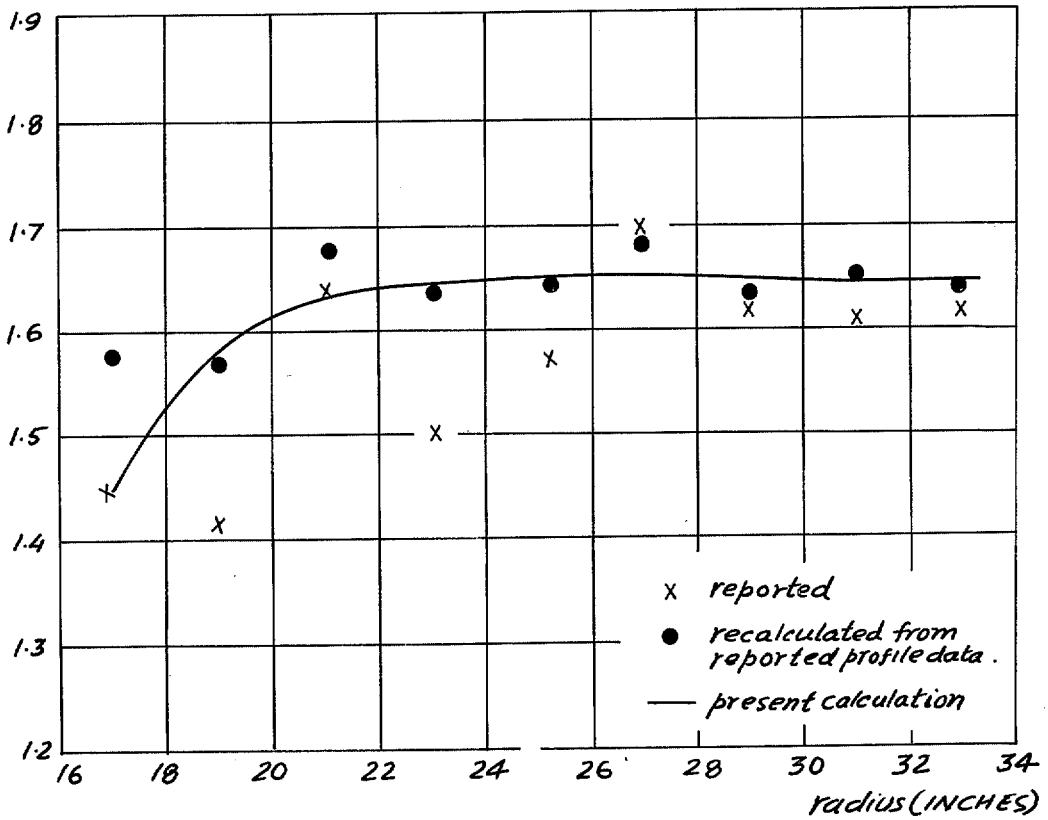

FIG. 10. Development of streamwise shape factor, Set 1.

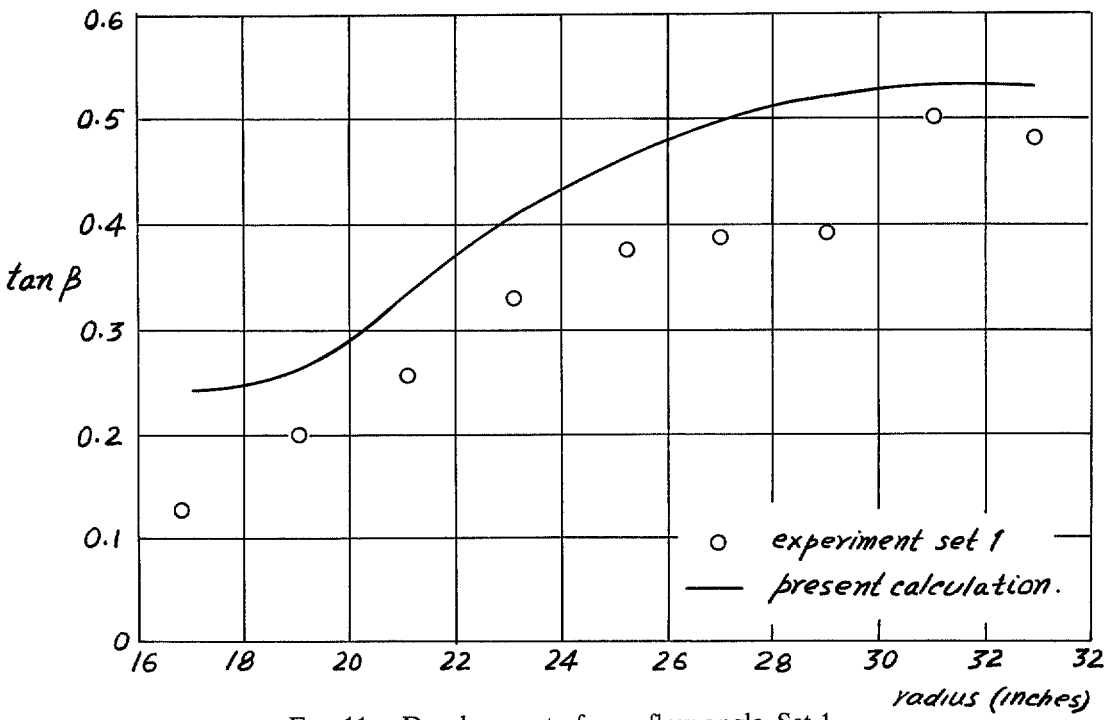

FIG. 11. Development of crossflow angle, Set 1.

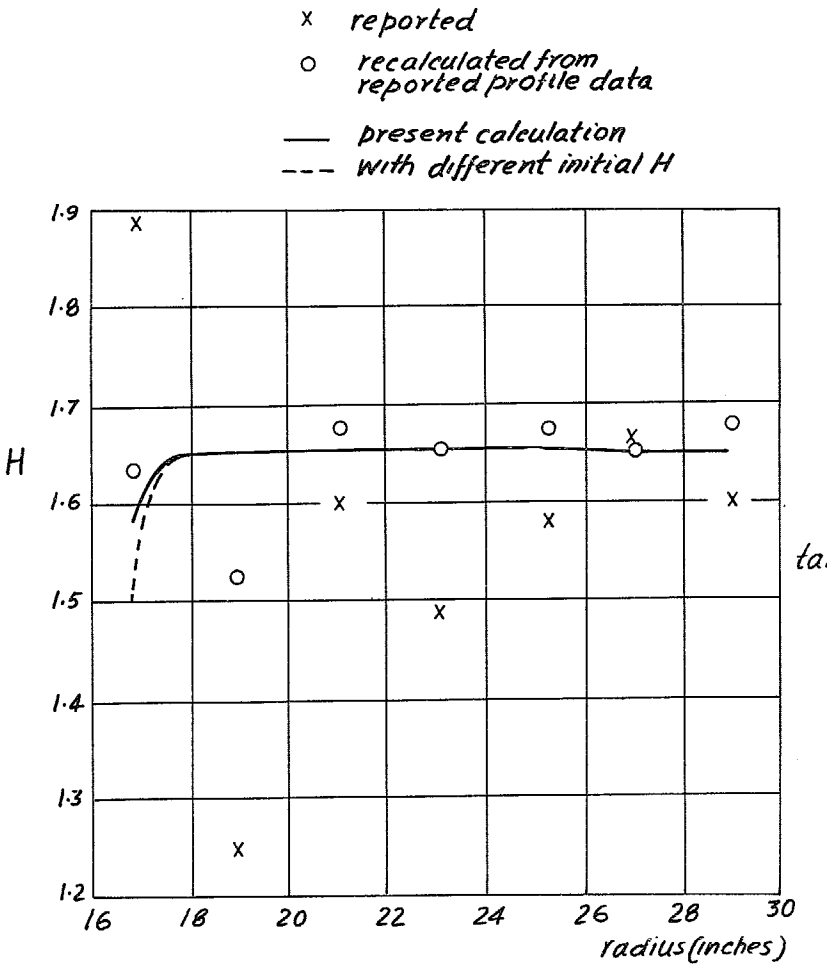

FIG. 12. Development of streamwise shape factor, Set 2.

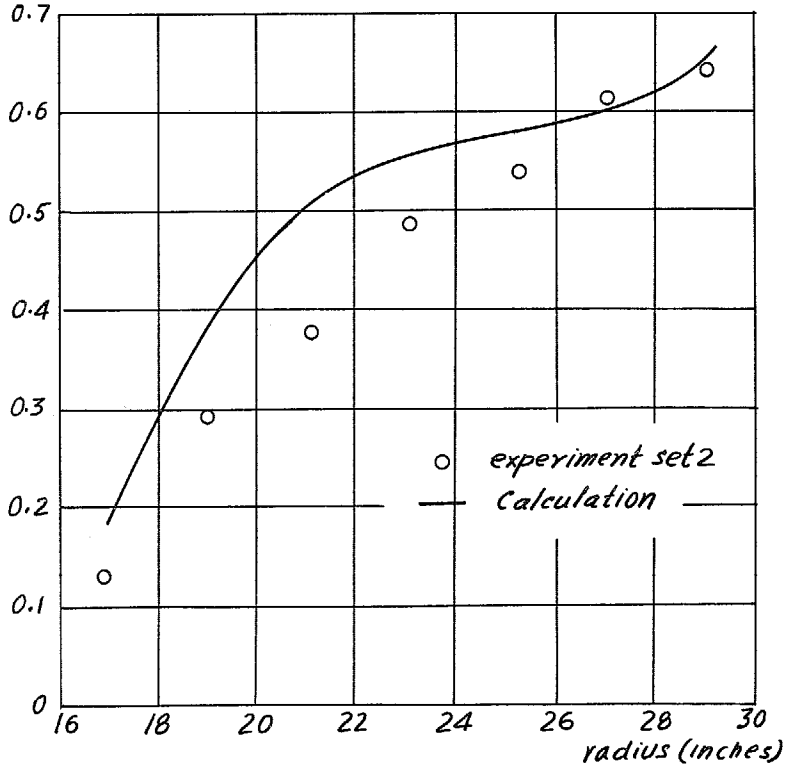

FIG. 13. Development of crossflow angle, Set 2.

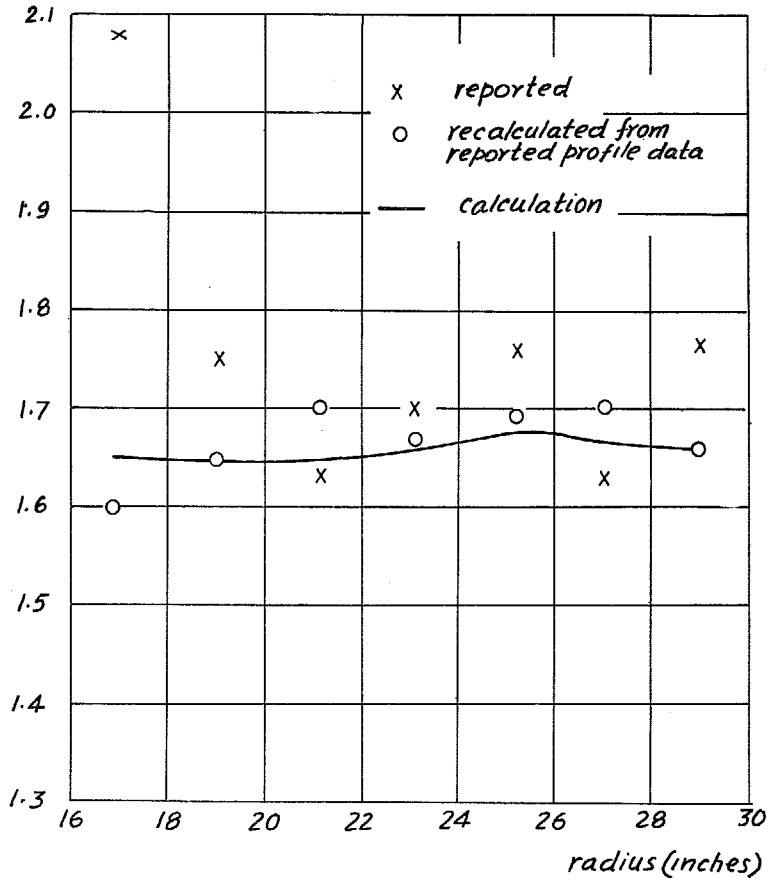

FIG. 14. Development of streamwise shape factor, Set 3.

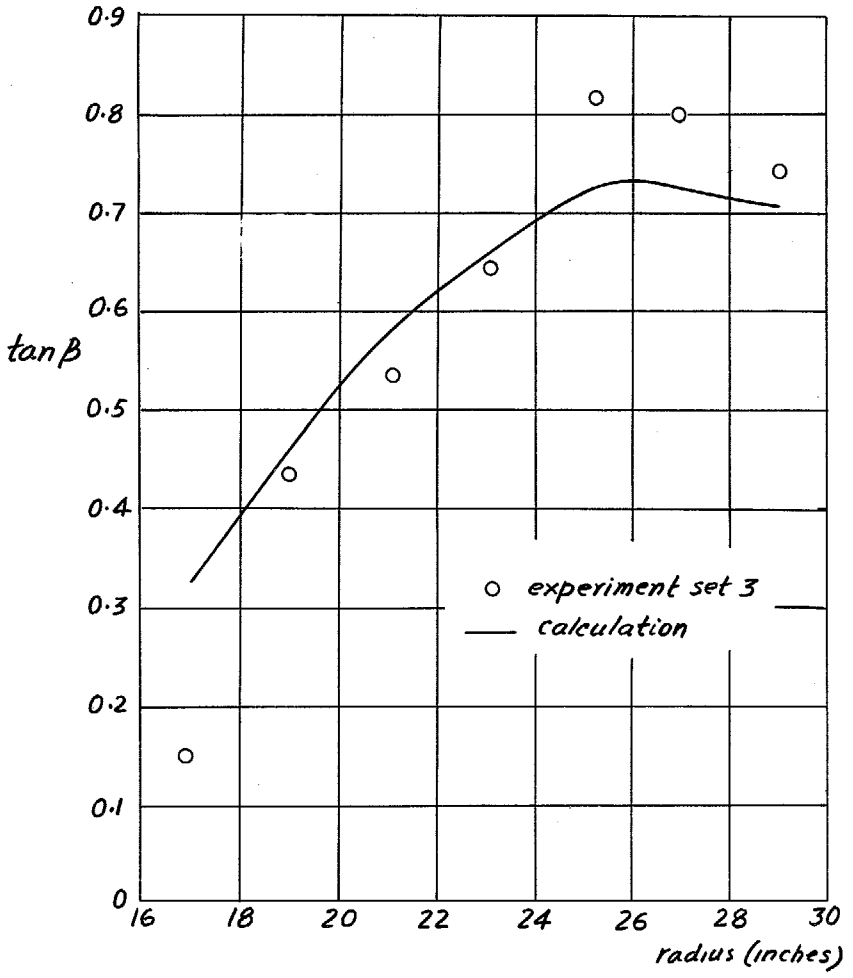

FIG. 15. Development of crossflow angle, Set 3.

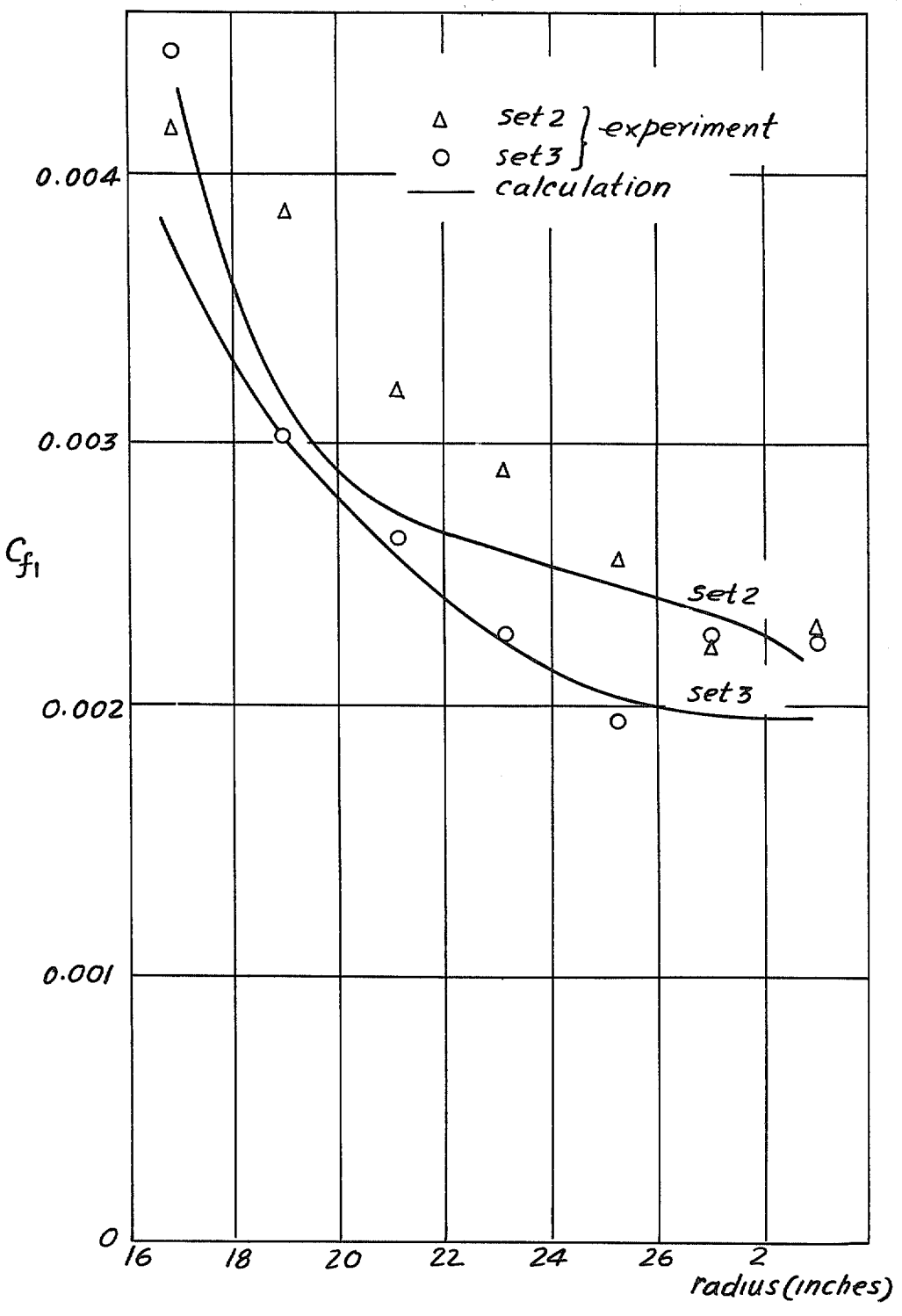

FIG. 16. Streamwise coefficients of wall shear stress.

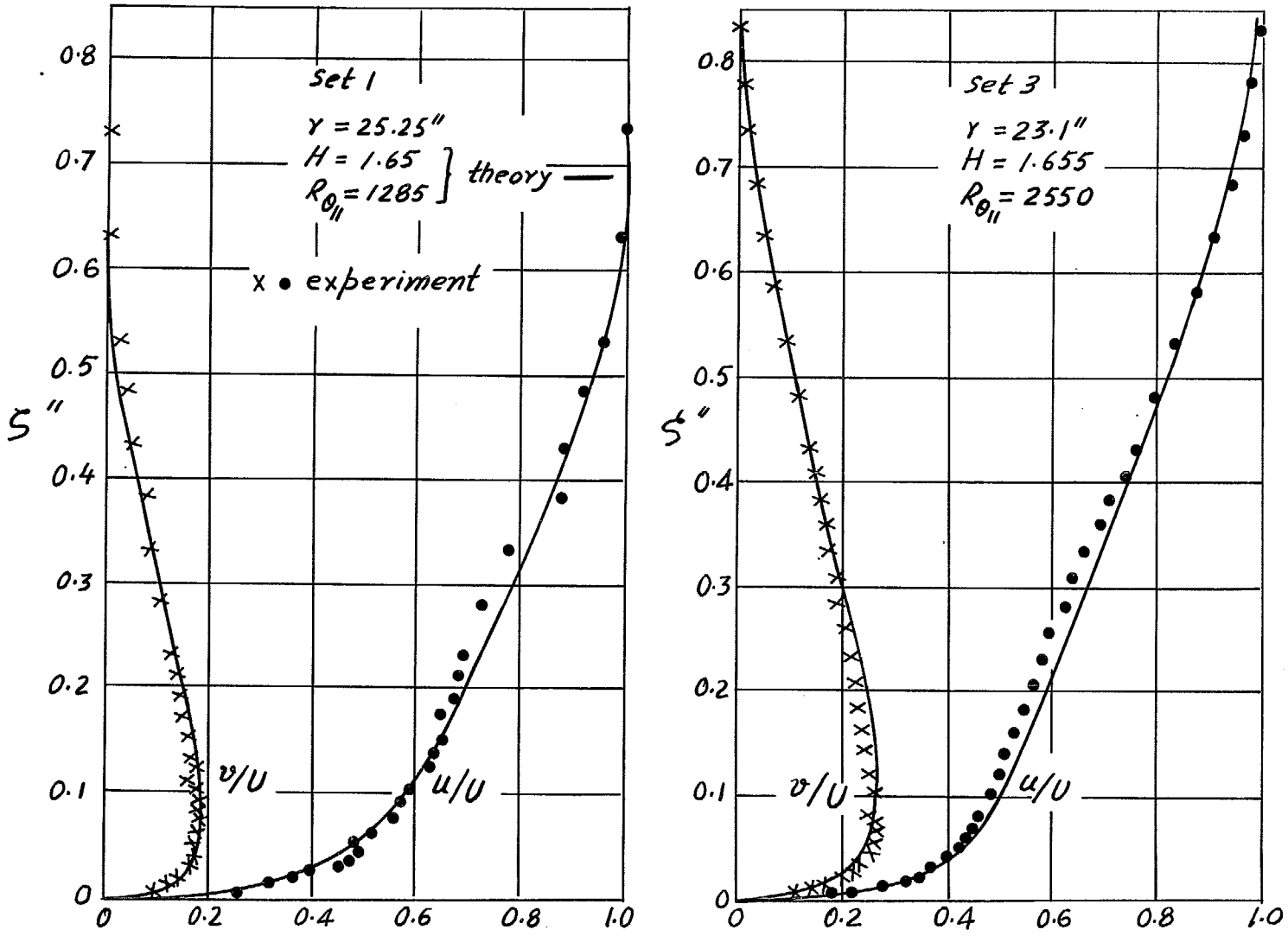

FIG. 17. Mean velocity profiles.

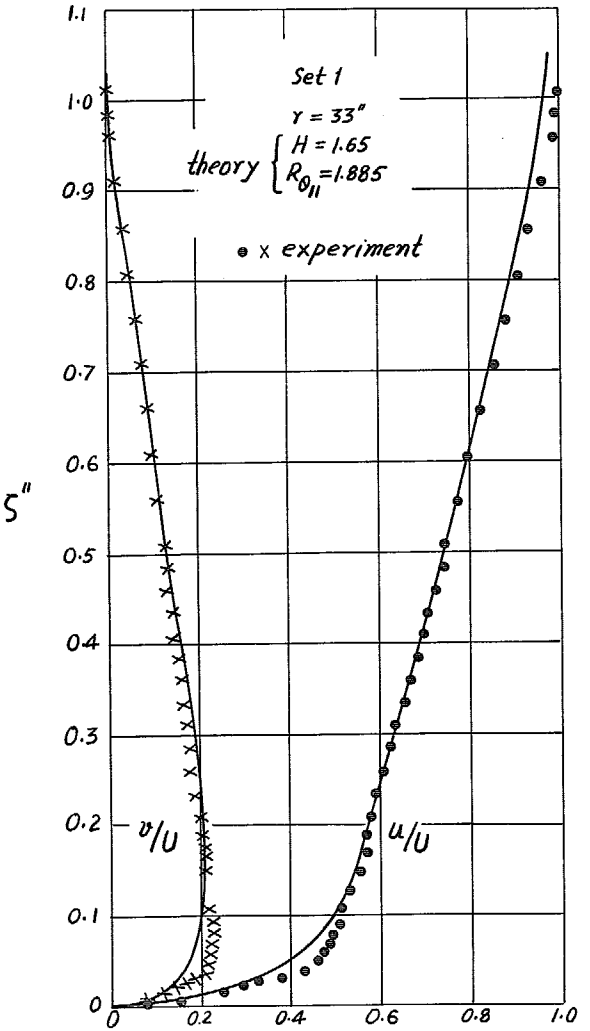

FIG. 18. Mean velocity profiles.

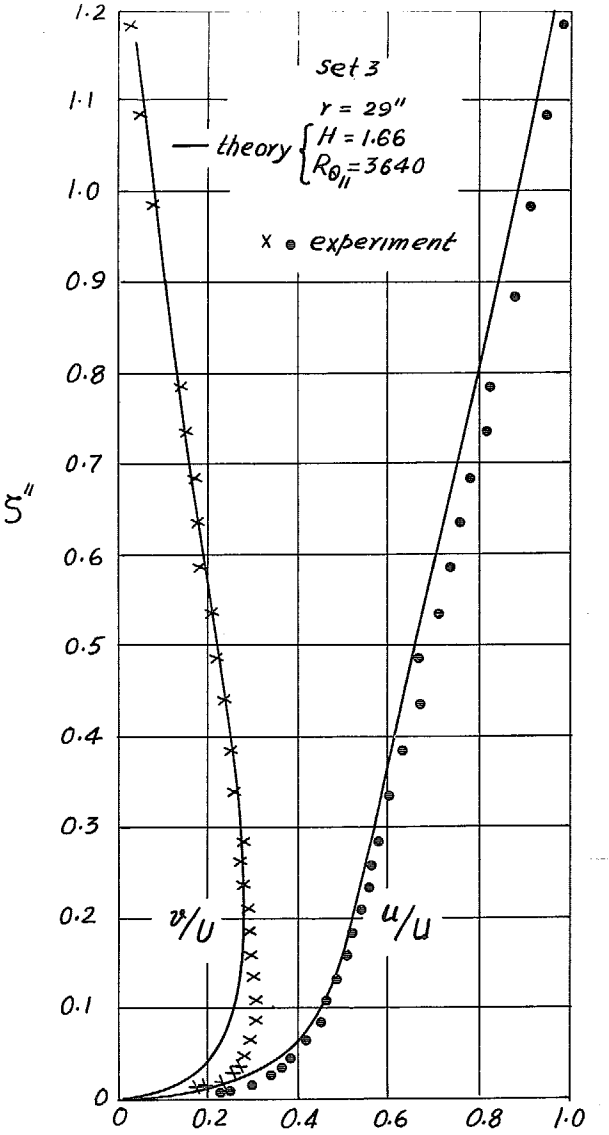

FIG. 19. Mean velocity profiles.

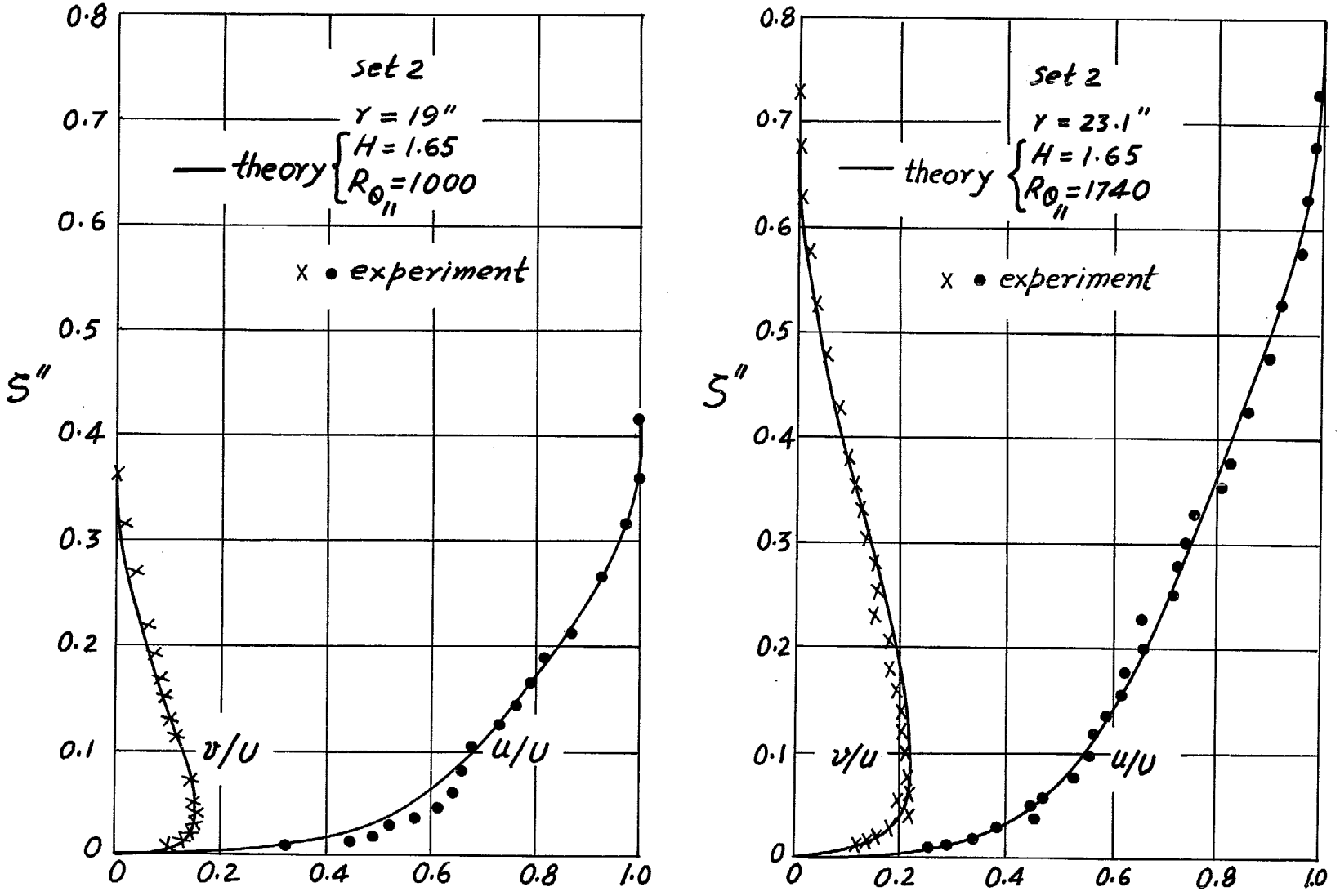

FIG. 20. Mean velocity profiles.

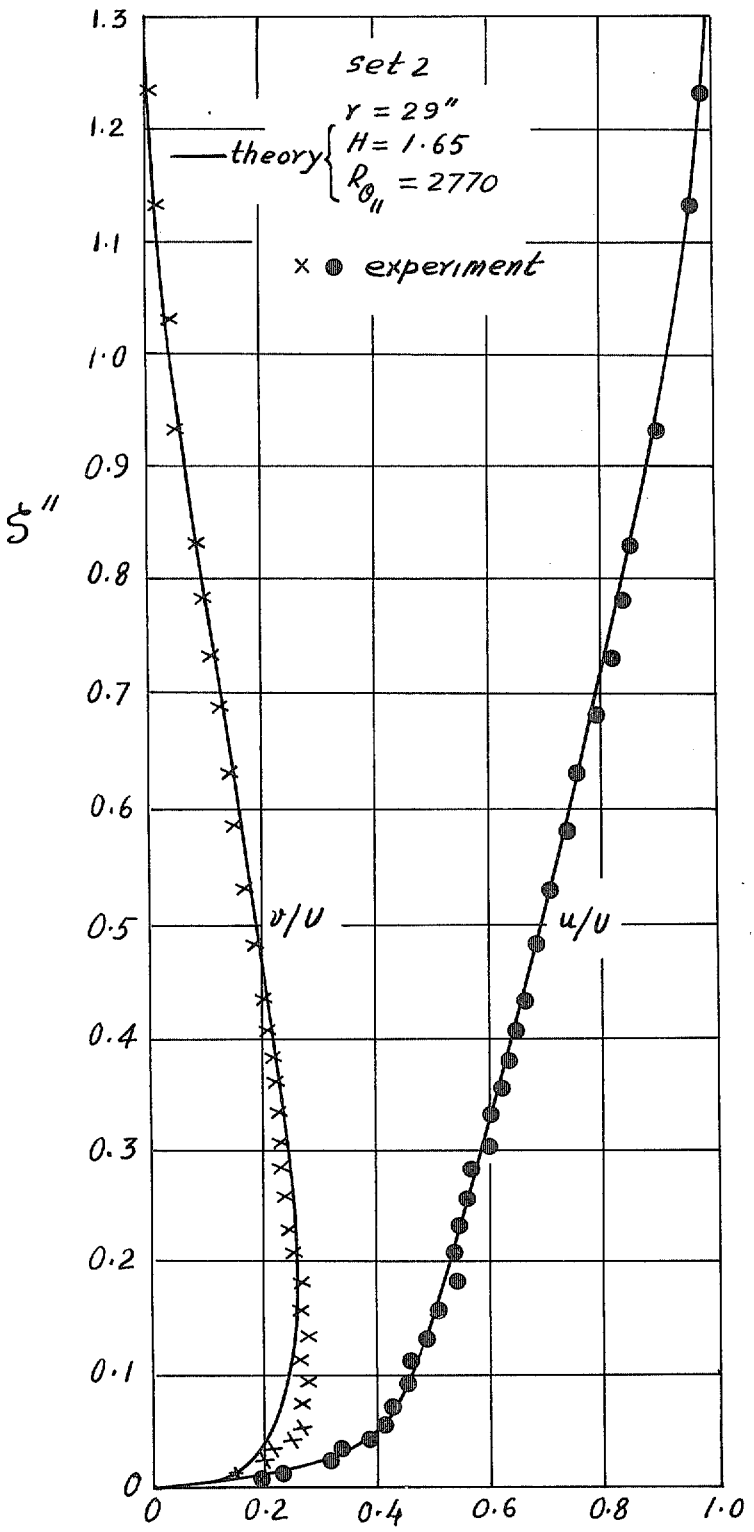

FIG. 21. Mean velocity profiles.

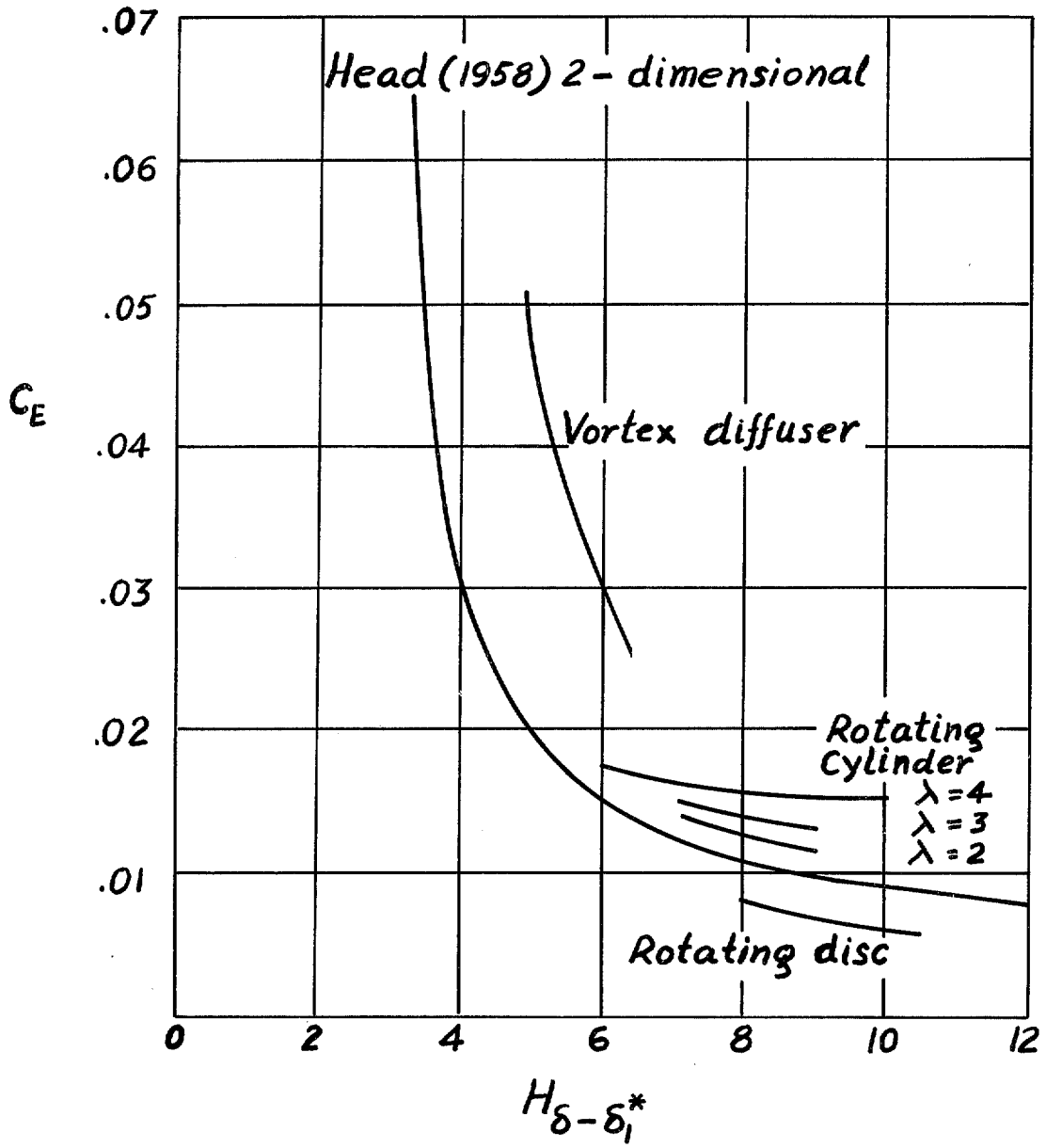

FIG. 22. Entrainment curves used in different calculations.

Printed in Wales for Her Majesty's Stationery Office by Allens Printers (Wales) Limited
Dd. 501372 K.5

Published by
HER MAJESTY'S STATIONERY OFFICE

To be purchased from
49 High Holborn, London WC1
13a Castle Street, Edinburgh EH2 3AR
109 St Mary Street, Cardiff CF1 1JW
Brazennose Street, Manchester M60 8AS
50 Fairfax Street, Bristol BS1 3DE
258 Broad Street, Birmingham 1
7 Linenhall Street, Belfast BT2 8AY
or through any bookseller

R. & M. No. 3646

SBN 11 470366 3